Available online at www.sciencedirect.com
SCIENCE DIRECT®
Journal of Solid State Chemistry 178 (2005) 521–535
JOURNAL OF SOLID STATE CHEMISTRY
www.elsevier.com/locate/jssc

Charge distribution and local structure and speciation in the UO_{2+x} and PuO_{2+x} binary oxides for $x \leqslant 0.25$

Steven D. Conradson[a,*], Bruce D. Begg[b], David L. Clark[a], Christophe den Auwer[c], Mei Ding[a], Peter K. Dorhout[d], Francisco J. Espinosa-Faller[a,e], Pamela L. Gordon[a], Richard G. Haire[f], Nancy J. Hess[g], Ryan F. Hess[a], D. Webster Keogh[a], Gerard H. Lander[h], Dario Manara[h], Luis A. Morales[a], Mary P. Neu[a], Patricia Paviet-Hartmann[a], Jean Rebizant[h], Vincenzo V. Rondinella[h], Wolfgang Runde[a], C. Drew Tait[a], D. Kirk Veirs[a], Phillip M. Villella[a], Franck Wastin[h]

[a]*Los Alamos National Laboratory, Chemistry Division, Materials Science and Technology Division and Nuclear Materials Technology Division, Los Alamos, NM 87545, USA*
[b]*Australian Nuclear Science and Technolgy Organisation, Menai, NSW 2234, Australia*
[c]*Commissariat a l'Energie Atomique, Marcoule, 30207 Bagnols sur Ceze Cedex, France*
[d]*Colorado State University, Fort Collins, CO 80523, USA*
[e]*Centro Marista de Estudios Superiores, Merida, Yucatan, Mexico*
[f]*Oak Ridge National Laboratory, Oak Ridge, TN 37831, USA*
[g]*Pacific Northwest National Laboratory, Richland, WA 99352, USA*
[h]*European Commission, JRC, Institute for Transuranium Elements, D-76125 Karlsruhe, Germany*

Received 3 June 2004; received in revised form 10 September 2004; accepted 16 September 2004

Abstract

The local structure and chemical speciation of the mixed valence, fluorite-based oxides UO_{2+x} ($0.00 \leqslant x \leqslant 0.20$) and PuO_{2+x}/$PuO_{2+x-y}(OH)_{2y} \cdot zH_2O$ have been determined by U/Pu L_{III} XAFS spectroscopy. The U spectra indicate (1) that the O atoms are incorporated as oxo groups at short (1.75 Å) U–O distances consistent with U(VI) concomitant with a large range of U displacements that reduce the apparent number of U neighbors and (2) that the UO_2 fraction remains intact implying that these O defects interact to form clusters and give the heterogeneous structure consistent with the diffraction patterns. The PuO_{2+x} system, which does not show a separate phase at its $x = 0.25$ endpoint, also displays (1) oxo groups at longer 1.9 Å distances consistent with $Pu(V+\delta)$, (2) a multisite Pu–O distribution even when x is close to zero indicative of the formation of stable species with H_2O and its hydrolysis products with O^{2-}, and (3) a highly disordered, spectroscopically invisible Pu–Pu component. The structure and bonding in AnO_{2+x} are therefore more complicated than have previously been assumed and show both similarities but also distinct differences among the different elements.

Keywords: Speciation; Local structure; X-ray absorption fine structure spectroscopy; Urania; Plutonia; Mixed valence actinide oxide; XAFS

1. Introduction

Crystallographically, i.e., based on their diffraction patterns that originate in the long-range average arrangement of atoms contained in the coherent parts of the crystal, the AnO_2 compounds display the fluorite structure for Pa–Cf [1]. In this, the O^{2-} ions form a lattice of cubes in which alternating cube-centers are occupied by the An(IV) ions. Each An(IV) is therefore surrounded by a cube of O^{2-} and the nearest neighbor environment for every O^{2-} is a tetrahedron of An(IV)

*Corresponding author. Fax: +1 505 665 8021.
E-mail address: conradson@lanl.gov (S.D. Conradson).

0022-4596/$ - see front matter © 2004 Elsevier Inc. All rights reserved.
doi:10.1016/j.jssc.2004.09.029

ions. The structures of these compounds are therefore relatively open and their densities relatively low because half of the cubes are empty.

If the AnO_2 compounds were inert and truly stable then not only would the technical issues involving them be easily resolved but they also would be of little scientific interest [2]. This is, however, not the case. Especially, when prepared from solution, many An ions in AnO_2-type materials coordinate OH^- ions (and possibly H_2O) that are only slowly expelled as the materials consolidate [3,4]. In addition, at least UO_2, [5] NpO_2, [6–9] and PuO_2 [10] are readily oxidized (and reduced) with concomitant addition (loss) of O atoms from the lattice [1]. In fact, x can be varied continuously over a range specific to each element, from as low as -0.5 (Pu) to $+1$ (U). The valence endpoint and most stable phase are highest for U and lowest for Pu, one manifestation of which is the fact that UO_2 readily oxidizes to higher forms in air whereas PuO_2 does not. AnO_2 may therefore often best be described as $AnO_{2\pm x}$, or even $AnO_{2+x-y}(OH)_{2y}\cdot zH_2O$. One of the more remarkable aspects of this behavior is that the basic crystallographic structure is mostly conserved for $-0.5\leqslant x\leqslant 0.5$ and beyond. Even as O atoms are added or removed, the diffraction pattern from the cubic An sublattice is retained except for changes of a few hundredths of an Å in its lattice constant that are the only indication the formation of the new, isostructural phases. For example, Pu_2O_3 is produced from PuO_2 by the sequential removal of every fourth O atom from the lattice. Similarly, 16 (or more) distinct phases have been identified between UO_2 and UO_3 that are all believed to be distinguished primarily by different, ordered arrangements of the O atoms that are (at lower x) adventitious to the original UO_2 structure, even while the U atoms undergo only minor displacements that conserve their symmetry [5]. Because of the stability of these putative phases relative to a random distribution of the extra O atoms or vacancies within the crystal, as oxidation occurs they form as clusters that coexist in the crystal with the original phase and grow and coalesce as the An:O ratio approaches the actual stoichiometry of the phase.

Based on both X-ray and neutron diffraction data, highly detailed descriptions of these phases and the structural mechanisms for their interconversions with the addition or loss of O atoms have been described for the UO_{2+x} system. The salient attribute of these mechanisms is that, consistent with the conservation of the U sublattice, the adventitious O atoms add through distortions and rearrangements of the O sublattice that tend to utilize the empty space of the unoccupied cubic sites. There is a long history for these models for UO_{2+x} $x\leqslant 0.25$, beginning with the "2:2:2" and "4:3:2" (referring to, respectively, O site vacancies and the numbers of O atoms displaced in [110] directions within chains and [111] directions that terminate chains)-type defects and chains [11–14] and more recently progressing to more extended clusters involving cuboctahedral, antiprism-type distortions of the original cubes [5,15,16]. The additional charge on the U ions in these models therefore tends to be somewhat dispersed rather than localized and is accommodated by small (<0.15 Å) reductions in some U–O bond lengths (balanced by expansions of others) and increases in the U coordination numbers. There are, however, three problems with these models, that most likely originate in the fact that diffraction is sensitive to the periodic components of the structure whereas local structure probes such as X-ray absorption fine structure (XAFS) spectroscopy and pair distribution function analysis see all of the atoms [17]. Conceptually, this delocalized charge distribution is inconsistent with both the known molecular and actinate [18–21] chemistry of the lighter actinides. In the former, the higher An valences exhibit multiply bound "oxo" groups at very short (<1.85 Å) An–O distances and lower total coordination numbers. In the latter, higher An charge is also stabilized with fewer O near neighbors and contracted bonds that may be divided into sets of longer and shorter ones [20–22] or be totally symmetric, e.g., KUO_3, [23] $BaUO_4$, [24] Ba_3UO_6 [19]. In this regard it is worth noting that while U_2O_5 and Np_2O_5 both have oxo groups (albeit bridging), the former compound has not been identified as an intermediate in the UO_2–UO_3 sequence but must be prepared by a different route [5]. Secondly, it is very difficult to determine the correct structures of disordered solids from diffraction data and the solutions to the fits of these patterns tend to be non-unique. Finally, whereas the oxidation of U and Np progress, respectively, to U(VI) and Np(V), PuO_{2+x} ceases oxidation at $x=0.25$ without exhibiting a separate phase that would account for the stability of this stoichiometry. This contradicts the tenet of thermodynamics that holds that a disordered material should not be a minimum in the total free energy surface.

Knowing the mechanism by which the O atoms are added and removed is essential because it is required for understanding and predicting the behavior of these materials. For example, the original description of PuO_{2+x} was accompanied by the speculation that the presence of the Pu(V) in PuO_2 would increase the solubility of this environmentally critical compound.10 Likewise, corrosion (and other chemical reaction) rates and their sensitivities to the presence of contaminants also depend on the intermediates that occur between the reactants and products. Fortunately, a direct probe for the chemical speciation and local structure of the An in $AnO_{2+x-y}(OH)_{2y}\cdot zH_2O$ independent of its long range order is available: XAFS spectroscopy [3,4,25,26]. This method has recently been used to characterize PuO_{2+x} [27–29] and UO_{2+x} [30] for $0.0\leqslant x\leqslant 0.25$.

2. Materials and methods

Preparation, handling, and characterization data for these samples as well as the details of the experimental measurements and data analysis have been reported in detail. For Pu, more than two dozen compounds prepared by a variety of methods including precipitation by both hydrolysis and heterogeneous reduction and gas phase oxidation with H_2O and O_2 were investigated [27,29,31]. Exact O stoichiometries in UO_{2+x} can be produced by controlling the O activity during firing and then confirmed via the diffraction pattern where the domains of the $UO_{2.25}/U_4O_9$ phase have a slightly different lattice constant than that of the original UO_2 [30]. All XAFS measurements were performed on end stations 4–2 and 11–2 at the Stanford Synchrotron Radiation Laboratory using a multielement Ge detector to obtain fluorescence mode spectra. Calibration of the energy was performed by measuring the spectrum of a Zr foil, either as part of the Pu spectrum or immediately before a Pu or U spectrum, and defining the energy of its first inflection point as 17999.35 eV. The accuracy of this method is ± 0.2–0.5 eV. All data were analyzed by standard methods. Curve-fits utilized amplitudes and phases calculated by the FEFF7 code [32]. The metrical results of the curve-fits for the nearest neighbor O shells are presented in Table 1. Those for compounds within a given class have been combined when the results were similar. In these cases the range is listed. Results for individual spectra contain an error that was derived by varying the parameter until the least squares error was higher than the best fit by 10% of the difference between this best fit and the fit without the shell in question (10% of the error for the contribution of the shell in question to the overall fit). As discussed in the next section, good fits often required two shells to fit the broad, anharmonic distribution of the O around the normal 2.33 or 2.35 Å Pu/U–O distance, when the separation between them was <0.13 Å then their weighted average distance was calculated and listed in the table along with the sum of the numbers of atoms in the two shells. Because of interference effects this sum is especially large when the separation was larger so that the numbers of atoms should be compared only for samples in the same class of compounds. Results for all spectra in which the 2.3 Å O shells were not combined and that also contain the U/Pu and second neighbor O shells have been reported [29,30].

3. Results and discussion

3.1. Homogenous $PuO_{2.0}$

The first finding based on a simple comparison of the spectra with the one calculated from the crystallographic structure is that simple, ordered PuO_2 is actually quite rare and is not produced simply by firing or calcining Pu compounds in air at very high temperatures (Figs. 1–3). Instead, it was serendipitously prepared during the attempted synthesis of KPu_2Se_6 by heating elemental Pu and Se and K_2Se_4 in a fused silica ampoule at 500 °C for 48 h [31]. The critical aspects of this preparation are the O potential controlled by the temperature of the O-reservoir of the silica container and the rigorous exclusion of any H_2O from the starting materials and during the entire time it was at high temperature (there may have been brief exposure during the preparation of the samples for the XAFS measurements).

3.2. Complex Pu–O distributions in conventionally prepared materials

The effects of not exercising control over these parameters are easily observed in the spectra from the other PuO_{2+x} samples. Disorder in the nearest neighbor O shell resulting from Pu–O bond that can be assigned to OH^- (An–OH bonds are contracted relative to other OR^- ligands [33,34]) and possibly H_2O ligands is not surprising in the materials prepared by precipitation (Figs. 2 and 4). "H_2O" would also include hydrogen bonded proton networks, giving Pu–O bond lengths differing from those found in solution and contributing to the asymmetric/anharmonic O distribution around the 2.33 Å principal crystallographic shell. Inclusion of protonated species in the initially formed precipitates would be expected, and their subsequent elimination and ordering of the lattice is undoubtedly related to the ripening process [4,35–38] that causes the solubility constants to change by orders of magnitude over time. These directly coordinated near neighbor O shells with shorter Pu–O distances are supplemented by longer Pu–O distances that result from the mirroring of these displacements on the neighboring Pu atoms. In terms of trying to classify the species that result from these extra O shells it is not practical to chemically distinguish H_2O and OH^- in these systems. When one occurs both are always at least potentially present because the O^{2-} ions can provide facile interchange via the reaction $H_2O + O^{2-} \Leftrightarrow 2OH^-$, where the proton transfer could be partial and the structure distorted because of hydrogen bonding.

What is unexpected, however, is that these additional shells of O atoms are also often found in materials prepared by oxidation at elevated temperature and even in ones prepared by firing at >1000 °C (Figs. 2 and 3). Either the rates of uptake of H_2O and its subsequent transport, hydrolysis, and coordination to Pu ions within the lattice are so high that quantities of it comparable to the amount of Pu present are taken up during cooling and subsequent storage under ambient conditions, or the Pu–OH^- bonds remain stable up to

Table 1
Pu and U nearest neighbor O metrical parameters

PuO_2 Crystal structure	*R*		2.336					
	N		8					
Ordered PuO_2 by chemical decompositon	*R*		2.33–2.34					
(Pu + silica rxn)	*N*		7.2–7.4					
	σ		0.076–0.077					
Pu–O distance near:	*< 1.9 Å*	*2.16 Å*	*2.32 Å*	*2.72 Å*	*2.8 Å*	*3.0 Å*	*3.1 Å*	*3.33 Å*
PuO_{2+x} prepared with high T processing								
High fired (a)			2.31 ± 0.02		2.76 ± 0.02	2.98 ± 0.02		3.27 ± 0.02
			5.8		1.7 ± 0.6	1.4 ± 0.6		0.4 ± 0.1
			0.050 ± 0.014		0.050 ± 0.016	0.050 ± 0.009		0.050 ± 0.006
PuO_{2+x} $x = 0.03$–0.21								
	1.85–1.91		2.32–2.35		2.71–2.81	2.94–3.02		3.30–3.33
	0.3–0.5		5.4–6.9		0.6–1.4	0.3–0.9		0.7–1.0
	0.050				0.051–0.076	0.051–0.076		0.051–0.076
$x = 0.26$	1.84 ± 0.02	2.13 ± 0.02	2.33 ± 0.01	2.73 ± 0.02		2.94 ± 0.02	3.19 ± 0.02	3.37 ± 0.02
	0.5 ± 0.2	1.0 ± 0.3	4.9	0.4 ± 0.2		1.1 ± 0.3	1.2 ± 0.4	0.4 ± 0.2
	0.050 ± 0.014	0.050 ± 0.014	0.055 ± 0.012	0.053 ± 0.015		0.053 ± 0.015	0.050 ± 0.015	0.050 ± 0.015
Corroded metal	1.93 ± 0.02		2.26 ± 0.02	2.74 ± 0.02		2.97 ± 0.02		3.27 ± 0.02
	0.4 ± 0.1		4.3	1.3 ± 0.4		1.9 ± 0.6		1.6 ± 0.5
	0.050 ± 0.015		0.106 ± 0.018	0.080 ± 0.014		0.080 ± 0.015		0.080 ± 0.015
Low fired			2.32 ± 0.02	2.68 ± 0.02	2.86 ± 0.02		3.07 ± 0.02	3.31 ± 0.02
			5.1	1.4 ± 0.4	1.6 ± 0.4		0.9 ± 0.2	0.4 ± 0.1
			0.050 ± 0.014	0.050 ± 0.011	0.055 ± 0.006		0.050 ± 0.004	0.050 ± 0.004
High fired (b)	1.88 ± 0.01		2.31 ± 0.02		2.78 ± 0.03			3.34 ± 0.01
	0.3 ± 0.1		5.9		0.7 ± 0.2			1.0 ± 0.3
	0.050 ± 0.015		0.081 ± 0.014		0.067 ± 0.011			0.067 ± 0.005
15% humidity	1.85 ± 0.02	2.14 ± 0.02	2.32 ± 0.02		2.81 ± 0.02			3.34 ± 0.02
	0.5 ± 0.2	1.6 ± 0.6	6.7 ± 2.0		0.3 ± 0.1			0.5 ± 0.1
	0.050 ± 0.015	0.090 ± 0.015	0.081 ± 0.013		0.050 ± 0.006			0.050 ± 0.005
37% humidity	1.89 ± 0.02	2.13 ± 0.02	2.32 ± 0.02	2.72	2.87		3.08 ± 0.02	3.32 ± 0.02
	0.6 ± 0.2	0.7 ± 0.1	6.3	0.2	0.5		0.4 ± 0.1	0.9 ± 0.2

	0.050±0.007	0.050±0.007	0.050±0.015	0.045	0.045		0.050±0.003	0.050±0.005
80% humidity	1.88±0.01	2.19±0.02	2.33±0.02		2.77±0.02			3.33±0.02
	0.7±0.2	2.1±0.3	5.8±1.7		0.2±0.1			0.7±0.3
	0.050±0.014	0.090±0.014	0.073±0.012		0.059±0.013			0.050±0.005
Aqueous PuO_{2+x} precipitates: hydrolysis	1.82–1.88	2.19–2.23	2.35–2.39		2.77–2.84	3.03–3.06		3.28–3.32
	0.4–0.6	1.5–3.1	3.4–5.0		0.3–0.9	0.6–1.3		0.7–1.3
	0.050±0.010	0.050–0.070	0.050–0.87		0.050–0.055	0.0500.098		0.044–0.054
Aqueous PuO_{2+x} precipitates: reduction with Fe	1.84–1.87		2.31±0.02		2.79–2.80	2.98–3.01		3.33–3.35
	0.4–0.7		6.8–8.5		0.5–0.7	0.4–0.5		0.5–0.9
	0.050±0.011		0.064–0.074		0.055±0.010	0.055±0.010		0.055±0.012
Fe + NaOCl			2.31±0.02		2.76–2.78	2.98–3.04		3.32–3.36
			7.6–8.0		0.5–0.6	0.3–0.4		0.8–1.2
			0.088–0.091		0.050–0.055	0.055±0.007		0.055±0.022
ERDA + Al	1.82±0.12		2.31±0.02		2.84±0.02	3.02±0.02		3.37±0.02
	0.2±0.1		8.0		0.6±0.2	0.6±0.2		0.1±0.0
	0.050±0.010		0.087±0.011		0.055±0.015	0.055±0.016		0.055±0.004
ERDA + Al + NaOCl	1.77±0.02	2.16±0.02	2.34±0.01		2.86±0.02	3.06±0.02		3.32±0.02
	0.2±0.1	1.4±0.4	5.1		0.6±0.3	0.8±0.3		0.4±0.1
	0.050±0.016	0.074±0.012	0.074±0.010		0.065±0.016	0.055±0.016		0.055±0.006
UO_2 Crystal structure	*R*		2.36					
	N		8					
U–O distance near	*<1.8 Å*	*1.95 Å*	*2.25 Å*	*2.38 Å*	*2.55 Å*	*2.77 Å*	*2.93 Å*	*3.16 Å*
UO_{2+x} $x=0$–0.05	1.73–1.74	1.94		2.36	2.58±0.01			
	0.4–0.5	0.5–0.6		6.5–7.6	0.5±0.2			
	0.045±0.018	0.045±0.010		0.074–0.076	0.045±0.005			
UO_{2+x} $x=0.08$–0.12	1.72–1.73	1.97–1.98	2.23–2.24	2.38	2.52–2.55	2.77±0.02	2.96±0.02	3.20–3.22
	0.3–0.4	0.6–0.7	1.9–2.1	3.2–4.2	1.2–1.6	0.7±0.2	0.6±0.1	0.6–0.8
	0.045±0.016	0.095±0.017	0.045±0.014	0.045±0.013	0.045–0.047	0.045±0.016	0.045–0.047	0.045±0.007
UO_{2+x} $x=0.17$–0.20	1.73–1.76		2.25–2.26	2.40–2.42	2.56±0.02		2.90–2.93	3.11±0.01
	0.3		1.8–1.9	1.9–2.6	0.8±0.3		0.5–0.8	0.6±0.2
	0.045±0.007		0.045–0.057	0.045–0.057	0.045±0.015		0.045±0.010	0.045±0.006

R = U/Pu–O distance, N = number of atoms in shell, σ = U/Pu–O pairwise Debye–Waller factor, "–" = range of results for multiple spectra/samples, "±" = uncertainty for single spectrum/sample or for multiple spectra that gave same result.

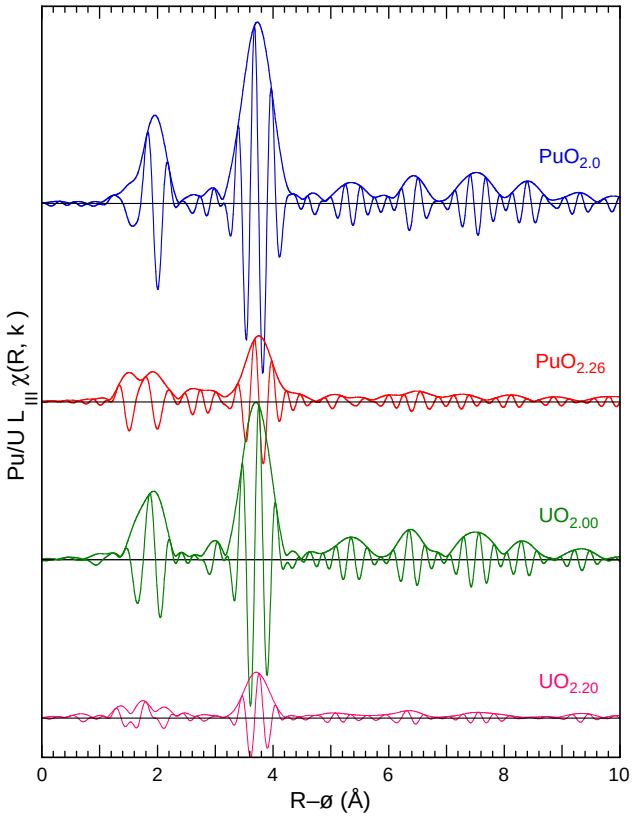

Fig. 1. Fourier transform moduli and real components of $k^3\chi(k)$ for indicated samples from $k = 3.0-14.7$ (Pu) and 2.7–15.0 (U) $Å^{-1}$. The spectra of the samples with $x = 0$ closely resemble those calculated from the crystal structure, with high amplitudes for the nearest neighbor O and Pu/U contributions, minimal non-crystallographic features apart from these, and features from the extended structure continuing through high R. The addition of O to near the An_4O_9 composition of the next phase eliminates the high R structure, substantially diminishes the amplitude of the Pu/U contribution without affecting its position or real component, and causes the nearest neighbor O contribution to split into several features at both lower and higher R than its original location.

these high temperatures. Whichever it may be, PuO_2 displays an extremely—perhaps uniquely—high affinity for H_2O. Furthermore, the narrower features and the much greater amplitude relative to the width of the nearest neighbor O peak in the $\chi(R)$ spectra of the

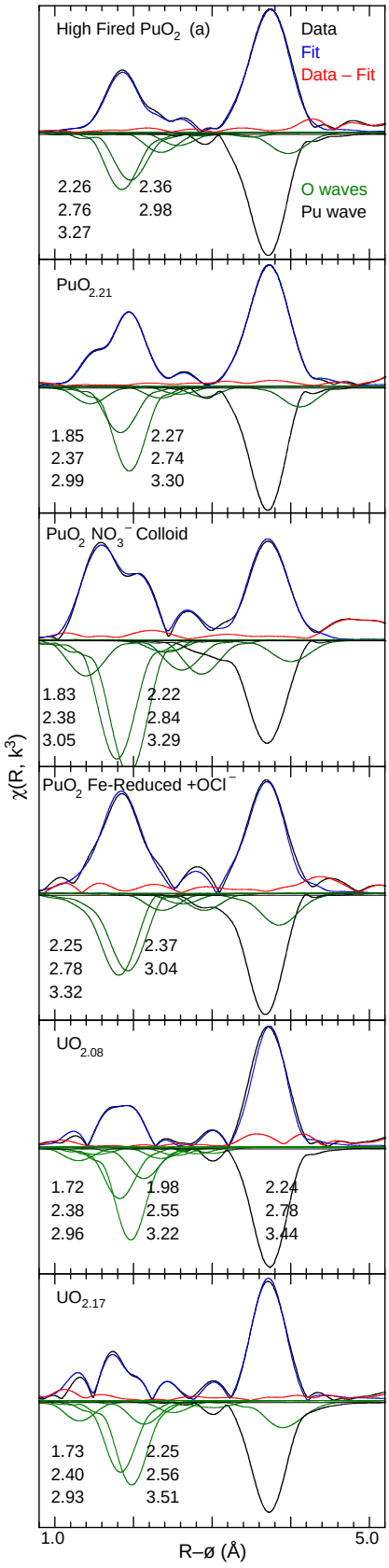

Fig. 2. Fourier transform moduli of $k^3\chi(k)$ from $k = 3–14$ $Å^{-1}$ of spectra, fits, difference, and (inverted) contributions of the individual O and Pu shells for indicated samples prepared by both oxidation with H_2O at elevated temperature and precipitation from aqueous solution by hydrolysis and heterogeneous reduction. The ordinates are not to the same scale. The Pu/U–O distances (in Å) are listed; the relative significance of these shells can be determined from the figures. Oxo groups associated with Pu(V) both occur and are absent for both types of PuO_{2+x} preparation methods and Pu–O distances associated with coordination with H_2O/OH^- are observed in varying amounts in the high temperature materials. A variety of U–O distances, including one corresponding to oxo bonding, also are found in $UO_{2.17}$.

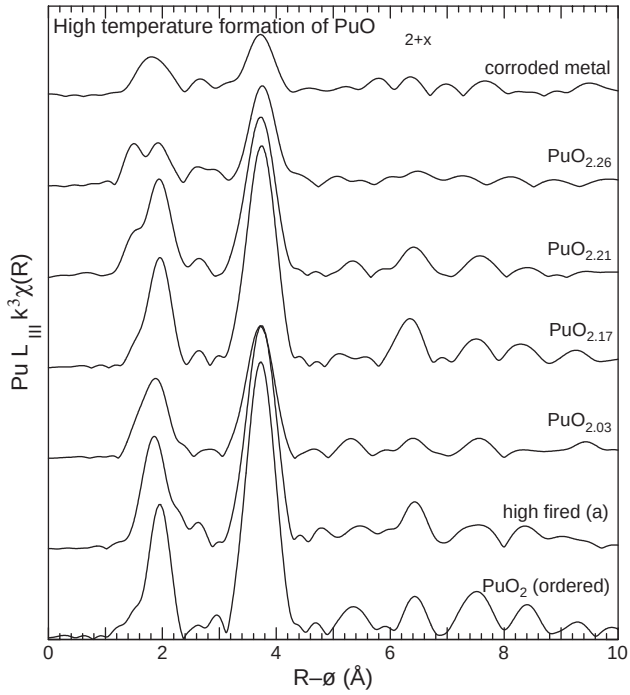

Fig. 3. Fourier transform moduli of $k^3\chi(k)$ from $k=3$–$14\,\text{Å}^{-1}$ of spectra for indicated samples prepared by oxidation with H_2O at elevated temperature. Relative to the ordered, crystallographic material, the nearest neighbor O contribution at $R=1.9\,\text{Å}$ can be complicated with features at both lower and higher R, the Pu contribution at $R=3.8\,\text{Å}$ retains its position and shape even while its amplitude can be substantially diminished, and the long range order indicated by the peaks at higher R also decreases in association primarily with the Pu. These characteristics indicate deviations from the crystallographic structure in terms of a multisite O distribution and single site but disordered Pu distribution. Although the O shells are found near the same distances in all samples when they occur, they do not always occur.

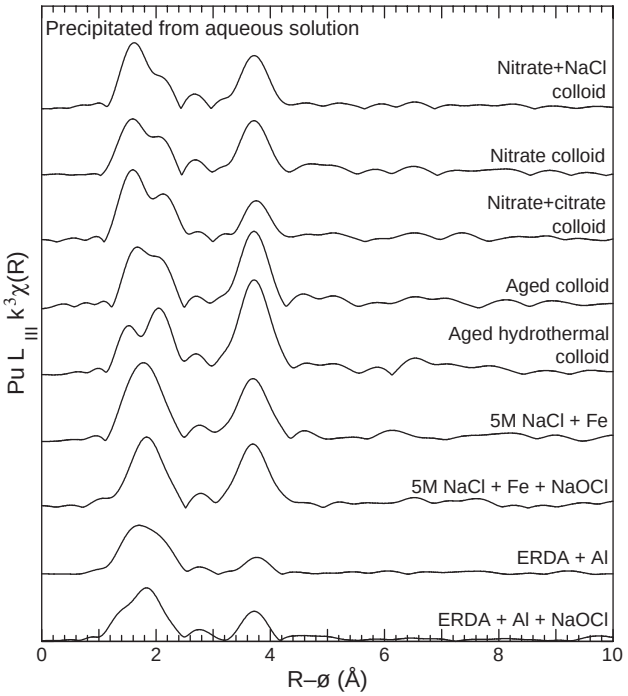

Fig. 4. Fourier transform moduli of $k^3\chi(k)$ from $k=3$–$13\,\text{Å}^{-1}$ of spectra for indicated PuO_{2+x} samples prepared by hydrolytic or reductive precipitation from H_2O (ERDA is a brine simulant). Consistent with the fact that most of these materials do not diffract, the features are smaller and usually broader than in the spectra from materials prepared at elevated temperature and there is no extended structure. The multiplicity of features for the nearest neighbor O contribution for $1.2<R<3.2\,\text{Å}$ is indicative of a multisite O distribution with the shells when they do occur at the same distances in all PuO_{2+x} type samples. The single peak of variable, low amplitude for the Pu contribution demonstrates that the Pu shell is disordered single site while retaining its original Pu–Pu distance. Precipitation therefore gives the same structural attributes as high temperature oxidation but results in less order.

compounds prepared at elevated temperature indicate a corresponding higher degree of local order in the Pu–O distributions in the compounds reacted at elevated temperature that is consistent with the expected annealing process. Remarkably, however, the Pu–O distances calculated by curve-fits of the extended X-ray absorption fine structure (EXAFS) region of the spectra are quite similar for both types of preparation, with shells near 1.85, 2.25, 2.35 (although the uniqueness of these two is apparently dependent on the preparation method), 2.8, 3.0, and 3.3 Å in almost all of the samples (Table 1). Not all of the samples display all of these shells in significant amounts, and the endpoint material, $PuO_{2.26}$, shows larger deviations and some additional shells. The corroded metal sample is also anomalous.

A caveat in using the exact distances is that, because of the challenge involved in unambiguously extracting them from materials that exhibit disorder as these do, the error is probably larger than the ± 0.01–$0.03\,\text{Å}$ expected and some with small separations may be artifacts from the disorder. Although curve-fits determine the optimum metrical parameters—distances, numbers of atoms, Debye–Waller factors—for a given model for the local structure around the absorber, they do not indicate whether the model in terms of the numbers and types of shells of neighbor atoms that define it is correct except in cases where two shells converge into a single one. XAFS thus also suffers from the general problem in structure analysis, that of uniqueness. For these PuO_{2+x} spectra the near neighbor, singly bound O region with $2.15\leqslant \text{Pu–O}\leqslant 2.45\,\text{Å}$ always requires at least two shells for an adequate fit, with one above and one below 2.3 Å. The 0.10–0.18 Å separation between these two shells is, however, at or below the 0.11 Å resolution limit of these data and is therefore not necessarily significant in itself but rather an indication of an anharmonic distribution that is better fit with the extra freedom pertaining to additional shells even when constrained then with a simple Debye–Waller factor [29,30].

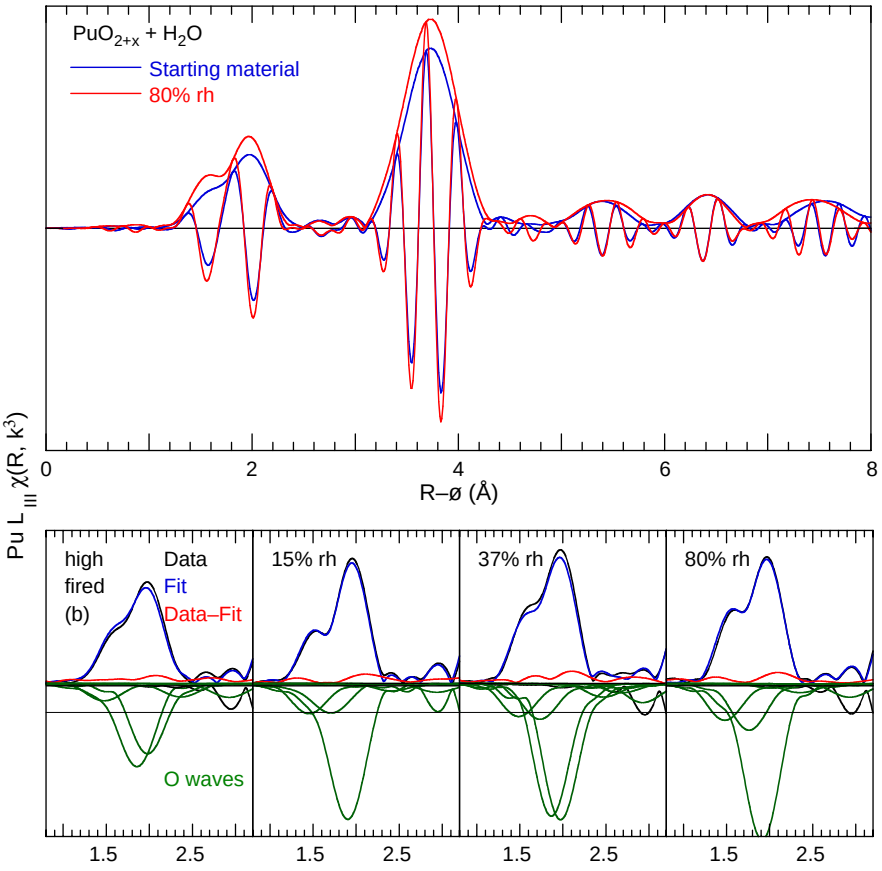

Fig. 5. Fourier transform moduli (and real components, upper) of $k^3\chi(k)$ from $k = 3.1$–$14.8\ \text{Å}^{-1}$ of spectra and (lower) fits, difference, and (inverted) contributions of the individual O shells for samples prepared by equilibrating the high fired (b) sample at the indicated relative humidities at ambient temperature. This particular material, although displaying a prominent contribution from an oxo shell, exhibits an unusually low amount of O with Pu–O distances longer than the 2.35 Å of the ordered, crystallographic structure as well as significant extended structure and a high amplitude for the Pu contribution. Although the spectra of the reacted samples are unique in requiring an O shell near 2.15 Å for a good fit and there is some inconsistency in the necessity for two O shells around 2.25 and 2.35 Å, the feature at $R = 1.5$ Å and corresponding amplitude of the oxo shell is unequivocally larger after exposure to H_2O vapor and then (compare against reference line) continues to increase slowly but monotonically as the relative humidity increases.

The separations between these two shells differ slightly but consistently depending on the method of preparation. Most of the materials prepared at elevated temperatures that are better fit by two shells display a 0.10 Å separation between the one with a Pu–O distance falling at <2.3 and the other at >2.3 Å. Because of this small separation the value listed in Table 1 is the weighted average; which almost always falls very close to 2.32 Å for these samples. (The exception is the corroded metal where it is significantly shorter.) The difference between these two distances is at or very close to 0.16 Å for the hydrolytically prepared colloids, which often exhibit a shoulder or even resolved peak in this region of the $\chi(R)$ spectra. These are therefore reported as two distinct shells at a higher and lower distance. Finally, the reductively prepared colloids display a separation of around 0.13 Å. These have also been combined to give a Pu–O distance of 2.31 Å.

In addition, the fits to some spectra—notably the series reacted with H_2O vapor at ambient temperature (Fig. 5) that are also similar to each other in displaying (vide infra) well developed and resolved oxo shells—are significantly improved by including a third O shell in this region. In these cases, the short Pu–O distance is decreased to <2.15 Å, one remains between 2.25 and 2.30 Å, and the longer one shifts somewhat higher. The short distance is similar to that observed in symmetric actinates.

What these problems show is that the result that should be emphasized is the overall distribution function described by the curve-fits and not the precise values of the parameters determined by them [29,30]. Nevertheless, the commonality of the general aspects of the curve-fits results indicate that the bond lengths are largely determined by the type of ligand, as is typical of coordination chemistry of molecular complexes. In fact, the Pu–O bond lengths found by curve-fits of the XAFS data are so similar to those in coordination compounds that they can be assigned to specific ligands based on these distances; OH^- for the shorter Pu–O distance

$\leqslant$2.25 Å, O^{2-} between 2.25 and 2.35–2.40 Å, and H_2O beyond 2.35 Å. (A table of nearest neighbor distances for a large number of valences, ligands, and coordination geometries is available [31].) This scheme is not necessarily rigorous; the 2.4 Å distance could also reflect a variety of particular bridging geometries for fractionally protonated ligands and the bond length elongation that normally accompanies them.

3.3. *Pu XANES and local geometry*

There is another feature in the XAFS spectra in addition to the Fourier transform peak widths that distinguishes compounds subjected to elevated temperatures (including the hydrothermally treated ones) from those that have not. The amplitudes of the principal absorption peaks in the XANES are always lower than that of ordered PuO_2 for the high temperature materials (Fig. 6), although the area of the peak is at least somewhat conserved by a concomitant increase in the width of this feature that shifts the inflection point energy somewhat lower. Compounds that have never been exposed to high temperature exhibit the converse effects. If the XANES of ordered PuO_2 was at one extreme then it would be easy to associate the spectral behavior with the degree of local order, but since it is bracketed by the two types of spectra this cannot be the case. Insofar as the XANES also depends on local geometry and the differences between the $\chi(R)$ spectra that reflect the structure of the two classes of compounds are less than the differences between the spectra of the individual samples within a class, this distinct difference in the XANES is difficult to understand. A speculative explanation would be that the two types of XANES correlate with a difference in stereochemistry from a less to a more stable local conformation that does not effect the one-dimensional information in $\chi(R)$ but does modify the XANES.

3.4. *Speciation of adventitious O in PuO_{2+x}*

Although the simple coordination reactions with H_2O and the species formed as a result is of interest insofar as it may differentiate Pu from other actinides and influences, e.g., solubility and H_2 evolution, the primary issue in PuO_{2+x} remains the disposition of the added O. The critical sample in determining this was $PuO_{2.26}$. The nearest neighbor O region in its $\chi(R)$ spectrum shows two clearly resolved peaks of relatively low but similar amplitude; the Pu–O nearest neighbor distribution is obviously more complicated than the single O shell of the ordered, crystallographic structure (Fig. 1). The peak at lower R, whose large relative amplitude clearly points to its origin in a structural feature, also occurs almost 0.6 Å below the O peak in the spectra from the ordered PuO_2 samples. Curve-fits (not shown, but cf. Fig. 5 for similar examples) show that these two peaks require four shells to be completely fit. Vis-à-vis the previous discussion of the limitations of the curve-fitting process, three of these correspond to singly bound O ligands, with overlapping Pu–O distances of 2.13, 2.28, and 2.41 Å that give an almost uniquely broad O distribution. This in turn implies some novel aspects of the structure at the O saturation limit. The fourth shell, completely resolved from these others and essential in fitting the lower peak in $\chi(R)$, has a Pu–O distance of 1.84 Å. Bond lengths this short in both molecular complexes and extended solids are found only for the

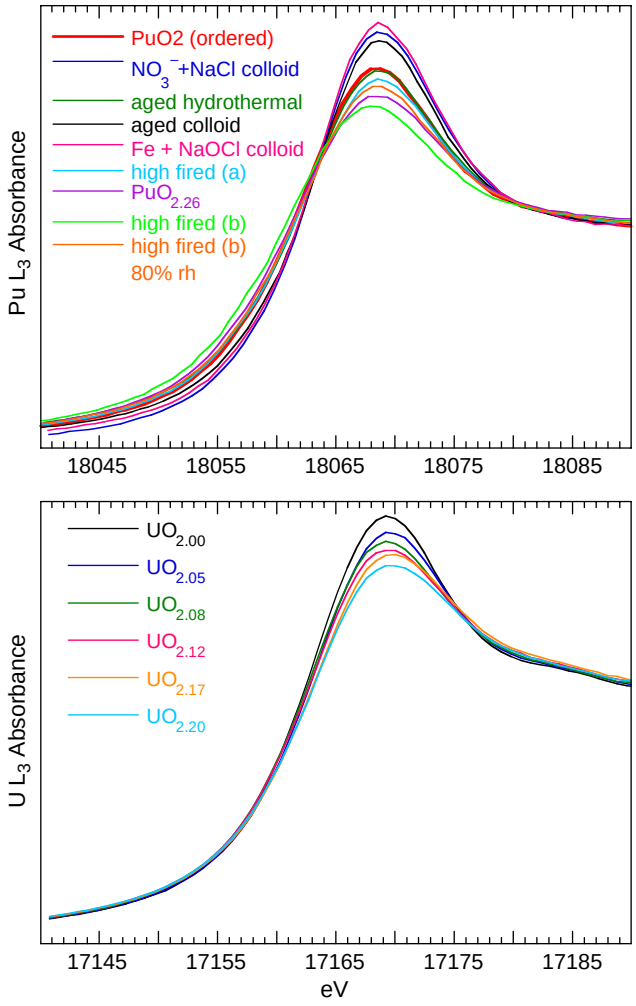

Fig. 6. L_3 absorption edges for indicated PuO_{2+x} and UO_{2+x} samples. PuO_{2+x} compounds precipitated from aqueous solution exhibit a higher, narrower peak than that of ordered PuO_2, whereas those prepared at elevated temperature display a lower, broader peak. There is no correlation of this behavior with the number of oxo atoms. The possible correlation with the degree of order is destroyed by the fact that the peak of ordered $PuO_{2.0}$ falls in between these two classes. It is possible that, in addition to order, this pattern results from a stereochemical difference. In contrast, increasing O stoichiometry in the spectra of UO_{2+x} causes a monotonic decrease in peak height and an increase in peak energy.

multiply bound oxo groups associated with valences $\geqslant$(V). Oxo groups can be defined as O shells with multiply bound An (V, VI, VII)–O with An–O distances $\leqslant$2.0 Å that usually impose additional constraints on the overall An geometry. This identification of their presence in $PuO_{2.26}$ demonstrates that an O shell near this distance should be included in the basic structural model used in the curve-fits. The application of this model shows that, although many samples attain good fits to their EXAFS spectra with either zero or negligible numbers of oxo atoms, many others require it even when their spectra do not display a resolved peak in $\chi(R)$. A more detailed inspection of this region shows that there are trends, especially in the real component of the transform, by which the presence of an oxo shell can be inferred directly from the spectra without resort to curve-fitting, further corroborating its presence. That the adventitious O in PuO_{2+x} is incorporated as oxo groups analogous to those in the higher valence molecular species is therefore unequivocal. If this feature in $\chi(R)$ originated in a multi-electron resonance above the edge [4] then (1) it would give a much more consistent number of atoms that correlated with the amplitude and width of the feature from the next shell and (2) it would not give a good fit with the Pu–O amplitude and phase because it would be a single feature and not an actual Pu–O wave in the k-based spectrum. The critical advantage in this study is the sample of $PuO_{2.26}$, whose structure allows the Pu–oxo wave and its characteristics vis-à-vis the fit to be examined separately.

3.5. Pu XANES and charge

One question about these oxo groups is the charge distribution and whether they are associated with Pu(V), (VI), or possibly both. One gauge of this is the bond length. In molecular complexes, Pu(VI)–oxo distances are almost always less than 1.8 Å and Pu(V)–oxo ones are longer. The Pu–O distances found in these materials are 1.82–1.92 Å. Although this is a relatively broad range, it is nonetheless in the regime expected for Pu(V). Another source of information is the XANES. The higher charge typically associated with higher metal valence increases the binding energy of the probed core electron and shifts the XANES upwards [29]. However, because of the higher covalency of the oxo group, the XANES of Pu(V) is actually shifted somewhat lower than that of Pu(IV), with the spectra of Pu(VI) compounds higher again. These energy shifts are modified by the details of the speciation, but it is true that for the same number of oxo groups a Pu(IV/V) mixture should give XANES energies at or slightly below those of homogeneous PuO_2 whereas a Pu(IV/VI) mixture should result in a significantly higher energy. One trend, the ca. 0.1 lower peak height of the XANES relative to that of ordered PuO_2 for the heat treated materials (Fig. 6) and 0.15 higher amplitude for ones prepared from solution and its correlation with the peak width and the inflection point energy, has been described. Using the peak energy instead of the inflection point, the spectra from the set of compounds made from the same starting material and reacted at high temperature shows a negligible -0.1 ± 0.2 eV shift relative to ordered PuO_2, whereas the shift displayed by a second set is $+0.6\pm0.5$ eV. The peak energies of materials prepared by precipitation is only $+0.2\pm0.2$ eV. In attempting to identify the source of these shifts and its relation with the Pu valence, there is no correlation of these energies with the numbers of oxo atoms found by the curve-fits. This not only indicates that the shifts originate in a different phenomenon, but also implies that the peak energy of the XANES of the Pu–oxo species must be very similar that of ordered PuO_2. It is therefore approximately halfway between those typical of Pu(V) and (VI) species. The expanded Pu–oxo bond lengths relative to Pu(V) are symptomatic of lower covalency, which would tend to raise the Pu charge and XANES energy. The Pu associated with the oxo groups is therefore most like Pu(V), although with a less covalent oxo bond and somewhat higher charge than when this group occurs in molecular complexes.

3.6. Redox acitivty of PuO_{2+x}

The compounds studied also provide some information on the chemical reactivity of these Pu(V) oxo species. Their presence in the compounds prepared by hydrolytic precipitation shows that they are sufficiently stable to form under ambient conditions as well as at elevated temperature. This is further corroborated by a set of samples using the same starting material equilibrated with air with different amounts of relative humidity (Fig. 5). Even in the spectra themselves, increased humidity is easily observed to correlate with increased amplitude of a shoulder or resolved peak near $R=1.5$ Å on the low R side of the main O peak. Curve-fits show that this can be attributed to an increase in the number of O atoms with a Pu–O distance near 1.88 Å. At least for certain configurations of PuO_{2+x}—this material was notable for very low numbers of O atoms between 2.5 and 3.5 Å and a high degree of order in the principal O shell that resulted in relatively short (2.13–2.19 Å) Pu–O distances in fits where the total number of O atoms was constrained—oxo groups are not only stable under mild conditions but also reach equilibrium with the environment throughout the crystal in a finite length of time. Another anomaly in the reactivity is the effect of added OCl^-, which promotes oxidation of Pu(IV) to Pu(VI). Although OCl^- did retard the initial precipitation rate it had no effect on the final efficiency of the reduction. It was also associated with lower numbers of oxo groups in the precipitates,

more consistent with a kinetic effect on the formation of Pu(V). Finally, the presence of significant quantities of Pu(V) oxo groups in materials precipitated from aqueous solution demonstrates that the solubility of these sites is not enhanced nor increases the overall solubility of the solid and corroborates the stability of the mixed valence phase.

3.7. Implications and consequences of oxo speciation; collective behavior and nanoscale heterogeneity

The inconsistency in the enhanced stability of the disordered, mixed valence form of PuO_{2+x} without any indication of phase separation, while fascinating, nevertheless poses a conundrum in our ability to understand this compound. A starting point may be that two independent, state of the art, electronic structure calculations both place the adventitious O in the interstitial site formed by the empty O^{2-} cube and do not find oxo group formation [39,40]. This contradicts these EXAFS measurements; a 1.9 Å Pu–O distance places the O within the O^{2-} cube already occupied by a Pu ion. Since the accuracy of these calculations is known to be high, the error most likely resides in the relatively small number of atoms they can utilize. I.e., the interstitial site may be most stable in a PuO_2 crystal only a few dozen atoms in size, but evidently it is not in real materials containing much larger numbers of atoms. In large crystals comprised of many unit cells cooperative and collective effects—which include entropy as statistical behavior is initiated—can be important. An example of the first parts is the incorporation of adventitious O into UO_{2+x} as $UO_{2.25}$-type clusters. The microscopic structural attributes identified by the EXAFS in the PuO_{2+x} series also exhibit such effects, with the addition that the disorder suggests that entropy in combination with different types of bonding may be a significant factor.

These must, however, be inferred because the EXAFS data does not give direct information on nanoscale ordering. Although there are exceptions, the most common An(V, VI) structural motif is the trans dioxo geometry, in which there are two oxo groups on opposite sides of the An ion with bond angles that deviate only very slightly from 180°. Between four and six atoms reside in the plane through the An normal to this axis with the oxos, coordinating the An at distances 0.4–0.8 Å further than the oxos to form an oblate bipyramid. It is possible to devise scenarios for incorporating this geometry in the PuO_2 lattice. The easiest is placing the adventitious O atoms midway between two Pu ions, so that they reside on the midpoint of a 100 vector of a PuO_8 cube. The Pu–O bond lengths in this half the Pu–Pu distance, 1.91 Å, which is longer than those found in molecular complexes but actually quite close to those found in many of these samples and may be consistent with the bridging mode of this configuration. The four O atoms at the vertices of the (110) square normal to the dioxo axis automatically reside in the equatorial plane of the complex, and the remaining four either are the source of the oxo groups or must be displaced to non-bonding distances, perhaps towards the adjacent interstitial sites. The collective effect here is direct, each inserted oxo group is bonded to two Pu ions so that a [110] chain is obligatory.

A second configuration forms oxo groups from the two O atoms opposite each other in the [111] direction. In this case they are displaced towards the central Pu ion and are terminal rather than bridging, which has some advantages because increasing the overall O stoichiometry with oxo group formation requires the formation of more isolated complexes and bonding modes as the average Pu coordination number decreases. The remaining six O atoms alternate between being above and below the equatorial plane and so would be expected to either move into it or away from the Pu to a non-bonding distance. The cooperativity here is that these displacements result in some of the O atoms moving to positions <2 Å from the neighboring Pu ions, so that additional oxo groups again result, this time forming asymmetric bridges. The essential aspect of the modeling is that it demonstrates that, within the crystal, the formation of an oxo group on a particular Pu ion necessarily results in the formation of additional oxo groups on neighboring Pu's and that this sequence propagates through the crystal to form chains, filaments, or other types of clusters containing the Pu(V)–oxo moiety.

These models assume conservation of the Pu sublattice, which follows from the diffraction results that show disorder but not the formation of a new phase. This result is largely true for the EXAFS as well. Whereas, relative to the crystal, the O shell forms a multi-site distribution with the O atoms organized around a set of specific Pu–O distances, there is no evidence for any new Pu–Pu distances or significant shift from the crystallographic Pu–Pu distance. The loss of amplitude in the Pu–Pu contribution in the $\chi(R)$ spectra originates in small increases in the Debye–Waller factor reflecting a similarly small increase in the width of the pairwise Pu distribution but primarily in a reduction in the overall number of Pu atoms found in this shell using the harmonic approximation for this distribution. Modeling shows that this result requires a separation of the Pu distribution into two components [30]. One of these is a Gaussian one centered at the distance and exhibiting the width found by the fits. The second part, which accounts for the diminution in the total amplitude and not just faster damping, must be glassy, with a relatively flat atomic density spread over several tenths of an Å. The poor coherence in such an arrangement of atoms would result in its being invisible in the

diffraction pattern, and the wide range of Pu–O near neighbor distances could also obviate the typical signatures of glassy materials in the diffuse scattering. It is also possible that these non-PuO_2 structures could exhibit some local order but their small size and aperiodic arrangement precludes diffraction from them. The preponderance of the oxo groups, as well as some of the H_2O, could therefore reside in domains of disordered material coexisting with more normal PuO_2, resulting in a material that is heterogeneous on the nanometer scale. The H_2O complicates the interpretation of the spectrum because of the disorder it introduces independently of the adventitious O and its distribution through the lattice renders it difficult or impossible to ascertain if phase separation is occurring.

3.8. UO_{2+x} experiments

It is essential to determine which of these local speciation and reactivity characteristics are unique to Pu and which may occur with other AnO_2 compounds. The issue of common behaviors for the AnO_2's across the row, or even just U, Np, and Pu is complicated: as described in the introduction, the maximum valence in binary oxides goes as U > Np > Pu whereas the stability of high valence An(VII) in molecular complexes is Np > Pu > U. This breakdown of the parallels between the coordination and solid-state chemistry also extends to their structures. The structural motif for U in (VI) in aqueous systems is the trans dioxo moiety with U–O distances <1.8 Å, whereas solids exhibit a wider range of geometries that conserve the average bond length, including the 2.0 Å one in U_3O_8 and related systems [41–43] and the symmetric 2.16 Å distance mentioned in the introduction. As already pointed out, however, these known structures with their short bond lengths are not consistent with the proposed cuboctahedral model for U_4O_9 and the next higher oxides either. The significance of PuO_{2+x} is that it points to a different mechanism for the incorporation of the adventitious O through the An_4O_9 phase that involves more conventional oxo groups and that is then at least a possibility for other elements, e.g., U.

We have performed XAFS measurements on a series of UO_{2+x} samples, with $0.00 \leqslant x \leqslant 0.20$. As described in the introduction, the presence of multiple, coexisting, ordered phases correlated with the O stoichiometry is well understood in this system, culminating in specific structural models for these phases and the mechanism of O addition. A specific problem with UO_2 is its propensity for oxidization by air, requiring greater care to maintain the original stoichiometry of the samples. Mishandling could therefore have given samples that were $UO_{2.0}$ in the core of the particles and oxidized on the shells, a macroscopically phase separated mixture that would give erroneous results because XAFS does not distinguish between homogeneous materials containing multiple species and mixtures. For this reason, the UO_{2+x} samples were maintained under inert gas during all phases of their preparation and encapsulation. The stoichiometry was confirmed by X-ray diffraction, which showed the expected increase in intensity of the slightly shifted pattern from the U_4O_9 phase as the O activity in the synthesis increased. The powdered samples were encapsulated in Stycast resin and shipped under inert atmosphere, a procedure that has been used successfully with air sensitive materials. The encapsulated samples were only exposed to air for a few minutes during their transfer to the cryostat, which was immediately evacuated and cooled with liquid N_2 [30]. The subsequent XAFS spectra are completely consistent with their expected, measured stoichiometries, with the $x = 0$ sample showing a very high degree of UO_2 crystallographic ordering followed by monotonic changes in the XANES and EXAFS as x increases. There are no indications of deviations of any of the samples from their analyzed composition. Furthermore, while the U–oxo distances found are compatible with the reported structures of UO_3 [44], they are much shorter than those for U_3O_8 [41–43] despite the fact that this mixed valence species should be the dominant form resulting from air oxidation at ambient temperature. The handling procedures, original analysis, encapsulation, and the spectra themselves all corroborate the stoichiometries assigned to the spectra.

3.9. Phase separation in UO_{2+x}

The phase separation into the endpoints of the reaction, UO_2 and U_4O_9, or at least the retention of UO_2 that was ordered on a length scale that was long for EXAFS, was corroborated in the EXAFS, where the high R features in $\chi(R)$ from the extended, ordered UO_2 structure all decrease linearly in concert with the near neighbor U and O contributions instead of faster at higher R as would occur if the order diminished evenly throughout the material (Figs. 1 and 2). It is easy to observe this phase separation because, unlike all of the PuO_2 samples except the rigorously anhydrous one, this set of UO_{2+x} samples shows no sign of H_2O incorporation. The $UO_{2.00}$ spectrum is essentially identical to the crystallographic structure and all of the changes are strictly correlated with the addition of the adventitious O. This higher affinity of PuO_2 than UO_2 for H_2O has also been produced in electronic structure calculations [19]. Although careful, anaerobic handling precluded the addition of H_2O after the synthesis of these compounds, in PuO_2 it is retained after firing if present in the starting material.

The curve-fitting results for the nearest neighbor O shells (Table 1) corroborate this phase separation scenario because they show a smooth transition in the

behavior of these O shells, with some disappearing and some reappearing as x increases. The number of O shells required for the best fits is actually a maximum for intermediate values of x because these spectra not only contain contributions from the shells that do not occur at the lower and higher x values but also a unique one. This last finding may reflect the interfaces between the UO_2 and U_4O_9 phases within the composition range where these interfaces involve the largest numbers of atoms because the endpoint structures are similar in quantity and their domains are small.

3.10. Speciation of adventitious O

The primary similarity with PuO_{2+x} is that addition of O to UO_2 also produces clear signatures of uranyl oxo groups (Figs. 1 and 2); for both elements O is incorporated with the formation of actinyl oxo complexes analogous to the higher valences in molecular complexes. For UO_2, this result contradicts 40 years of models based on diffraction measurements. However, the $\chi(R)$ spectra for higher x, analogous to those of PuO_{2+x}, unequivocally show a resolved peak at lower R that is comparable in amplitude to that of the O^{2-} contribution at high x where the disorder has substantially lowered the amplitude from the spectra near X = O. This behavior in the spectra themselves is especially important because of ambiguity in the curve-fits. Although good fits to the $UO_{2.00}$ spectrum are obtained with only the crystal structure, it is necessary to at least try the same basic structure with many shells in fitting all of the spectra. When this is done it is found that the fit for $UO_{2.00}$ is slightly improved when additional O shells are included (Table 1), including ones at 1.74 and 1.94 Å. Closer inspection and evaluation of these results, however, reveals that these very small, unresolved contributions to the fit are artifacts, most likely due to a combination of incomplete background subtraction and a small error in the calculated U–O phase and amplitude that is magnified because of the uniquely large amplitude of the U–O (2.36 Å) wave in the fully ordered material [30]. These shells at U–O distances <2.3 Å should therefore be disregarded for the low x values, whereas when they correspond to resolved features with amplitudes significant relative to the largest O feature in the spectra for higher x they are correctly interpreted as actual structural components.

Curve-fits demonstrate that the resolved low R feature in the spectra for $x \geqslant 0.08$ is well fit by an O shell with a U–O distance of around 1.75 Å. This is significantly shorter than the oxo distance in PuO_{2+x} and more consistent with U(VI) and the much greater stability of this higher valence to U(V) relative to Pu, where both valences are easily produced. The XANES is also more consistent with U(VI) (Fig. 6). The peak energy increases monotonically with increasing x by an amount that would be expected for U(VI) based on the XANES of U(VI) complexes. The inflection point energy is constant, but the peak amplitude is also diminished for higher x and the higher energies for the inflection point on the back side of the peak indicate that, as for PuO_2, the peak width can increase to compensate for reduced amplitude and keep the area constant. These short U–oxo distances are also unlikely to be bridging.

3.11. Additional deviations from the UO_2 structure

Analogous to PuO_{2+x}, the appearance of this new peak at low R that signifies the formation of uranyl oxo moieties with the addition of O is accompanied by the growth of other features at higher R that signify the concomitant formation of O shells with U–O distances >2.4 Å and a multisite U–O distribution. For these samples (and possibly for UO_2 in general), unlike PuO_{2+x}, these new O shells are not associated with the susbstitutional or hydrolytic addition of H_2O and so must reflect lattice distortions that occur in response to the formation of the oxidized species and, ultimately, become U_4O_9. Like PuO_2, these new shells do not occur at random locations but as sets that exhibit similar U–O distances for all values of x (Table 1), signifying specific chemical species within the lattice. For example, the 1.98 Å distance for intermediate values of x is close to the U-oxo-type distance in U_3O_8 and certain uranates. Since this shell disappears for $x>0.15$ it may be part of the interface between the UO_2 and U_4O_9 domains, diminishing in number as the fraction of U_4O_9 approaches unity. Insofar as several of these additional U–O distances differ from those found for the PuO_2 system it is likely that the specific structures in UO_{2+x} differ from those in PuO_{2+x}, consistent with their differing mechanisms for approaching the An_4O_9 endpoint. The separation between the two shells that form the principal feature with a U–O distance near 2.36 Å for $x>0.05$ is large, $\geqslant 0.15$ Å, so that they are reported as two rather than a single one at the weighted average distance. This is more like the aqueous than heat-treated PuO_{2+x} compounds.

Another characteristic similar to PuO_{2+x} is that the total U amplitude also decreases with increasing x. This is, in fact, much more certain for UO_{2+x} because the ability to precisely control the PuO_{2+x} composition has not yet been developed. This behavior has been shown to imply separation into one phase or structure where the U sublattice retains the UO_2 structure and a second one where it is glassy [30].

3.12. Lessons learned

The essential aspect of AnO_{2+x} for U and Pu is that in its oxidation the actinide displays the speciation that is analogous to isolated molecular complexes and

uranates and not the proposed unique ones derived from locating the adventitious O in the interstitial, cubic holes. The normal mechanisms for stabilizing the high valence complexes—large decreases in some An–O bond lengths to form oxo groups accompanied by a decrease in the total coordination number—are therefore in effect. Beyond this, however, the reactivities are not the same as in molecular complexes but instead appear dominated by collective effects that, for Pu, provide exceptional stability to this structure. Thus, although the O activity in combination with a continuous range of local An potentials results in a smooth progression of composition from AnO_2 to An_4O_9 for both U and Pu, U_4O_9 quickly separates as a crystallographically distinct phase whereas Pu_4O_9 remains indistinguishable from the PuO_2 lattice even at the endpoint when it is the compound. The U/Pu atoms are thus described by a dynamic energy landscape in which their potential is modified by the addition or removal of O atoms through relatively long distances, and it is their response to these dynamical aspects that differentiates the two elements. In addition, the Pu(V) oxo sites appear less water soluble than in molecular complexes and can form from Pu(IV) under conditions far too mild to oxidize mononuclear complexes. More detailed information on the structures, additional characteristics of the reactivity, the behavior of other actinides, and the origins of these effects await further study.

Acknowledgments

All experimental measurements were performed at the Stanford Synchrotron Radiation Laboratory, a national user facility operated by Stanford University on behalf of the US Department of Energy, Office of Basic Energy Sciences. Health physics support was provided by the Los Alamos National Laboratory chapter of the Seaborg Institute for Transactinium Science. This work was supported by the NNSA and OBES Division of Chemical Sciences under Contract W-7405 and (at Colorado State) DE-FG03-97ER14797.

References

[1] R.G. Haire, L. Eyring, in: K.A.J. Gschneidner, L. Eyring, G.R. Choppin, G.H. Lander (Eds.), Handbook on the Physics and Chemistry of Rare Earths, Elsevier, New York, 1994, pp. 413–505.
[2] C. Madic, Science 287 (2000) 243–244.
[3] J. Rothe, M.A. Denecke, V. Neck, R. Muller, J.I. Kim, Inorg. Chem. 41 (2002) 249–258.
[4] J. Rothe, C. Walther, M.A. Denecke, T. Fanghanel, Inorg. Chem. 43 (2004) 4708–4718.
[5] G.C. Allen, P.A. Tempest, Proc. R. Soc. London A 406 (1986) 325–344.
[6] J.A. Fahey, R.P. Turcotte, T.D. Chikalla, J. Inorg. Nucl. Chem. 38 (1976) 495–500.
[7] L. Merli, J. Fuger, Radiochim. Acta 66–7 (1994) 109–113.
[8] P.J. Pan, A.B. Campbell, Radiochim. Acta 81 (1998) 73–82.
[9] D.W. Efurd, W. Runde, J.C. Banar, D.R. Janecky, J.P. Kaszuba, P.D. Palmer, F.R. Roensch, C.D. Tait, Environ. Sci. Technol. 32 (1998) 3893–3900.
[10] J.M. Haschke, T.H. Allen, L.A. Morales, Science 287 (2000) 285–287.
[11] B.T.M. Willis, J. Phys.-Paris 25 (1964) 431–441.
[12] B.T.M. Willis, Acta Crystallogr. Sect. A:: Found. Crystallogr. 34 (1978) 88–90.
[13] B.T.M. Willis, J. Chem. Soc. Faraday Trans. 83 (1987) 1079–1081.
[14] A.D. Murray, B.T.M. Willlis, J. Solid State Chem. 84 (1990) 52–57.
[15] D.J.M. Bevan, I.E. Grey, B.T.M. Willis, J. Solid State Chem. 61 (1986) 1–7.
[16] F. Garrido, R.M. Ibberson, L. Nowicki, B.T.M. Willis, J. Nucl. Mater. 322 (2003) 87–89.
[17] A.J. Garcia-Adeva, D.R. Conradson, P. Villella, S.D. Conradson, J. Phys. Chem. B 107 (2003) 6704–6716.
[18] R. De Blieck, E. Van Cappellen, G. Van Tendeloo, S. Amelinckx, R. Gens, J. Fuger, J. Solid State Chem. 68 (1987) 375–378.
[19] E.H.P. Cordfunke, A.S. Booij, V. Smit-Groen, P. van Vlaanderen, J. Solid State Chem. 131 (1997) 341–349.
[20] L.R. Morss, J. Chem. Thermodyn. 34 (2002) 229–237.
[21] S. Van den Berghe, M. Verwerft, J.-P. Laval, B. Gaudreau, P.G. Allen, A. Van Wyngarden, J. Solid State Chem. 166 (2002) 320–329.
[22] E.H.P. Cordfunke, D.J.W. Ijdo, J. Phys. Chem. Solids 49 (1988) 551–554.
[23] P.G. Dickens, A.V. Powell, J. Mater. Chem. 1 (1991) 137–138.
[24] H. Appel, M. Bickel, S. Melchior, B. Kanellakopulos, C. Keller, J. Lessc. Met. 162 (1990) 323–334.
[25] D.J. Jones, J. Roziere, G.C. Allen, P.A. Tempest, J. Chem. Phys. 84 (1986) 6075–6082.
[26] S.D. Conradson, Appl. Spectrosc. 52 (1998) A252–A279.
[27] S.D. Conradson, B.D. Begg, D.L. Clark, C. Den Auwer, F.J. Espinosa-Faller, P.L. Gordon, N.J. Hess, R. Hess, D.W. Keogh, L.A. Morales, M.P. Neu, W. Runde, C.D. Tait, D.K. Veirs, P.M. Villella, Inorg. Chem. 42 (2003) 3715–3717.
[28] P. Martin, S. Grandjean, M. Ripert, M. Freyss, P. Blanc, T. Petit, J. Nucl. Mater. 320 (2003) 138–141.
[29] S.D. Conradson, B.D. Begg, D.L. Clark, C. Den Auwer, M. Ding, P.K. Dorhout, F.J. Espinosa-Faller, P.L. Gordon, R.G. Haire, N.J. Hess, R.F. Hess, D.W. Keogh, L.A. Morales, M.P. Neu, P. Paviet-Hartmann, W. Runde, C.D. Tait, D.K. Veirs, P.M. Villella, J. Am. Chem. Soc. (2004), in press.
[30] S.D. Conradson, D. Manara, F. Wastin, D.L. Clark, G.H. Lander, L.A. Morales, J. Rebizant, V.V. Rondinella, Inorg. Chem. (2004), in press.
[31] S.D. Conradson, K.D. Abney, B.D. Begg, E.D. Brady, D.L. Clark, C. Den Auwer, M. Ding, P.K. Dorhout, F.J. Espinosa-Faller, P.L. Gordon, N.J. Hess, R.F. Hess, D.W. Keogh, G.H. Lander, A.J. Lupinetti, M.P. Neu, P.D. Palmer, P. Paviet-Hartmann, S.D. Reilly, W.H. Runde, C.D. Tait, D.K. Veirs, F. Wastin, Inorg. Chem. 43 (2004) 116–131.
[32] A.L. Ankudinov, J.J. Rehr, Phys. Rev. B:: Condens. Matter 56 (1997) R1712–R1715.
[33] D.L. Clark, S.D. Conradson, R.J. Donohoe, D.W. Keogh, D.E. Morris, P.D. Palmer, R.D. Rogers, C.D. Tait, Inorg. Chem. 38 (1999) 1456–1466.

[34] C.W. Williams, J.P. Blaudeau, J.C. Sullivan, M.R. Antonio, B. Bursten, L. Soderholm, J. Am. Chem. Soc. 123 (2001) 4346–4347.
[35] G.R. Choppin, Radiochim. Acta 43 (1988) 82–83.
[36] G.R. Choppin, H.A. Bond, P.M. Hromadka, J. Radioanal. Nucl. Chem. 219 (1997) 203–210.
[37] Y. Xia, L. Rao, D. Rai, A.R. Felmy, J. Radioanal. Nucl. Chem. 250 (2001).
[38] W. Runde, S.D. Conradson, D.W. Efurd, N.P. Lu, C.E. Van Pelt, C.D. Tait, Appl. Geochem. 17 (2002) 837–853.
[39] L. Petit, A. Svane, Z. Szotek, W.M. Temmerman, Science 301 (2003) 498–501.
[40] R.L. Martin, P.J. Hay, personal communication.
[41] B.O. Loopstra, Acta Crystallogr. Sect. B: Struct. 26 (1970) 656.
[42] B.O. Loopstra, J. Inorg. Nucl. Chem. 39 (1977) 1713–1714.
[43] P. Jollivet, C. Den Auwer, E. Simoni, J. Nucl. Mater. 301 (2002) 142–152.
[44] B.O. Loopstra, J.C. Taylor, A.B. Waugh, J. Solid State Chem. 20 (1977) 9–19.